LETTERS IN BIOMATHEMATICS
**An International Journal**

RESEARCH ARTICLE

OPEN ACCESS

# Dynamics of Salt Transport from the Aralkum Desert

B.S. Tleumuratova[1], S.M. Mambetullaeva[1], Zh.Zh. Kublanov[1]

[1]Karakalpak Scientific Research Institute of Natural Sciences, 41 Berdakh Avenue, Nukus, Republic of Karakalpakstan, Uzbekistan, 230100

**ABSTRACT**

Salt aerosol emissions from the Aralkum desert are of significance to environmental and human health. The trends in wind transport of salt (WST) from 1961 to 2025 were modelled using Aral-61+. The model accounts for effects of desiccation of the sea, salt content within the exposed seabed, vegetative cover and wind patterns. Annual salt emissions increased from 0.7 Mt yr-1 (1961-1970) to 128.4 Mt yr-1 (2011-2020), 131.5 Mt yr-1 (2021-2025). Emissions have increased monotonically, however non-linearly, with a decrease in rate of increase in recent years. In 1990, the 20 kg ha-1 yr-1 dry deposition contour extended 150 km to the south and 500 km to the southwest, whereas in 2024 it extended 300 km to the south and 800 km to the southwest. Compared to scenarios without vegetation, a reduction in dry deposition was seen in 2025 (7.1%), however previous research has shown that salt emissions could be reduced by 15-20% depending on assumptions made. Sensitivity analysis demonstrates the relationship between emissions and dry deposition with respect to source strength and transport parameters. Comparisons between historical data were limited. Dry deposition does not represent total salt deposition. Intensifying precipitation is a theoretical mitigation method and does not show that WST has been reduced.

**ARTICLE HISTORY**
Received October 16, 2026
Accepted: November 19,2026

**KEYWORDS**
Aral Sea; wind-borne salt transport; salt deposition; soil salinization; mathematical modeling; phytoremediation.

## 1. Introduction

The desiccation of the Aral Sea—a large-scale environmental disaster—has drawn international attention for over half a century. Research into this phenomenon is of global importance, as it can inform evaluation of the consequences of salt lake desiccation observed worldwide, including Lake Urmia in Iran and the Salton Sea in California. Furthermore, Aralkum dust can be transported over substantial distances (Ge et al. 2022; Banks et al. 2022).

Researchers studying the Aral Sea crisis have identified wind-blown salt transport (WST) from the exposed seabed to surrounding areas as one of its most serious consequences because of its negative impacts on human health and the environment (Micklin 2004). Long-term exposure to fine particulate air pollution is associated with cardiopulmonary mortality and lung cancer (Pope 2002); however, this evidence does not establish carcinogenicity of Aralkum sulfate salts specifically. Health risks in the Aral Sea region require consideration of exposure, particle composition and other contributing factors (Wæhler and Dietrichs 2017). Transported over vast distances, salt plumes can contribute to soil salinization on irrigated lands and suppress vegetation cover (Novitskiy et al. 2024). Deposition of light-absorbing particles on snow and ice may influence glacier melt, and aerosol deposition may affect water quality in glacierized catchments (Yapiyev et al. 2021; Skiles et al. 2018). Further research is needed. The WST effects are a major issue within the Aral Sea region, and Central Asia as a whole. If action can be taken quickly, worsening of air quality and associated health implications may be prevented.

A new dynamic geostructure that has emerged in place of the Aral Sea—a combination of residual water bodies and exposed seabed—contains extensive surface and subsurface salt deposits (Kurbaniyazov 2017) and serves as a major source of large-scale salt and dust storms (Fig. 1).

**CONTACT** B.S. Tleumuratova

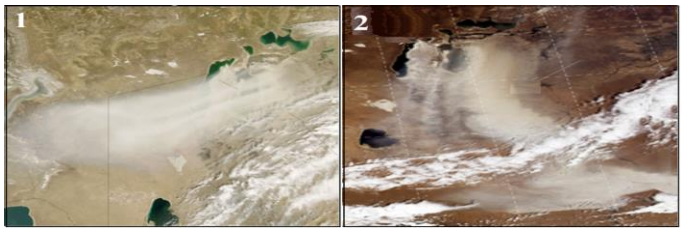


Fig. 1. Dust storms with salt transport in the southwestern (1) and southern (2) directions. Satellite imagery; original image provider, acquisition dates and reuse attribution require author confirmation.

Salt export from the exposed seabed of the Aral Sea represents a distinctive phenomenon in its scale and underlying surface dynamics. Other desiccating salt lakes, such as the Salton Sea in California, also generate dust from exposed shorelines (Parajuli and Zender 2018). In the Aralkum, WST emission sources constitute a dynamic, discrete array of puffy and crusty-puffy solonchaks. The chemical composition, particle size distribution and environmental impacts of the transported material are also important characteristics.

The crisis-driven evolution of the Aral Sea geostructure and its exposed seabed dictates the nonlinear nature of ongoing processes, complicating the study and forecasting of WST. Environmental forecasting is essential for medium- and long-term economic planning. In the Southern Aral Sea region, an agricultural territory, a key component of predictive analysis is the dynamics of the WST impact zone, which contributes to soil salinization and vegetation degradation. Assessing trends in the volume and transport distance of salts from the Aralkum requires a rigorous analysis of long-term WST dynamics and its underlying drivers.

As evidenced by a review of available publications from 1984 to 2025, the current state of knowledge regarding WST from the exposed seabed of the Aral Sea remains insufficient for identifying long-term process trends. The literature review on wind-borne transport of soil material from the Aralkum presented below reveals a wide discrepancy in estimates of WST volume and transport distance.

For instance, Mozhaitseva and Nekrasova (1984) calculated that, during that period, an average of 60 to 100 t/ha of salts were emitted into the atmosphere annually. Azydova and Semenov (1985) estimated the total emission capacity of the Aral aerosol source at 20–30 million t/year, including 200–300 thousand t/year of salts. Rubanov and Bogdanova (1987) showed that the export of water-soluble salts alone,—excluding the terrigenous component of dust storms,—reached 43 million t/year. According to Razakov and Kosnazarov (1987), salt export from severe solonchaks on the exposed seabed ranged from 12 to 20 t/ha annually. Chub (2000) noted that 53 million tons of salts were exported annually from the water surface, 57 million tons from the exposed seabed, and 13 million tons from solonchaks.

Solid particles originating from the Aral Sea basin can be transported over several hundred or even thousands of kilometers, reaching Georgia, Central and Eastern Siberia, and the Arctic regions of Russia (Micklin 2007; Singer et al. 2003; P. Micklin 1988). Dust from the Aral Sea basin can also extend northwest to Belarus and Lithuania, and southeast to Afghanistan (Goudie and Middleton 2006). However, quantitative data regarding the specific transport distance of *salts* from the Aralkum in these studies are virtually absent.

Uncertainties are greatest in locating sources of salt. Identifying locations of salty/salt-affected areas within the exposed seabed has proven challenging, due to dynamic changes in the location of these areas as a result of retreating shorelines and large scale deflation events. Remote sensing techniques have been used to locate sources of dust emissions (Xi and Sokolik 2016; Nobakht et al. 2021). However, cloud cover can severely restrict satellite observations of dust emissions (Xi et al. 2025). Thus, observations of dust events are lacking in continuity (Wang et al. 2022). Furthermore, because a continuous satellite record is not available for the study period (1961-2025), and separation of salt content within exported sediments is difficult, WST cannot be reconstructed at a long term scale using satellite data alone

.Similarly, ground-based monitoring studies of dry atmospheric salt aerosol deposition—typically covering only 2–3 decades (Tolkacheva 1995; Kosnazarov 2005)— provide limited insight into long-term WST dynamics. Exposed dust traps in open-wind settings frequently collected salts of non-Aral origin, such as those transported from the Garabogazköl lagoon.

The scientific value of studies relying primarily on qualitative methods is indisputable, as foundational monitoring of specific WST aspects provides essential empirical data. However, their spatiotemporal non-representativeness hinders the direct application of qualitative findings for developing scientific frameworks for effective planning, strategy selection, and decision support regarding WST mitigation.

The interrelationships between WST, water salinity, exposed seabed soil salinity and plant community dynamics motivate a systems-level analysis of long-term WST. Tleumuratova (2018) developed MIDACS (Macromodel of Influence of Drying Aral on Climate and Salinization) to assess ecosystem transformations and their influence on soil and climatic conditions. Earlier numerical studies of salt aerosol transport and its environmental effects (Tleumuratova 2009, 2018) provided a basis for regression approximations of soil salinity, vegetation cover and salt transport. Máté et al. (2017) modeled shelterbelt influences on wind erosion, and Li et al. (2022) examined dustfall and heavy metal exposure in a saline lake basin.

Mathematical modeling and systems analysis provide a means to reconstruct long-term WST dynamics. This study focuses on estimating

the salt fraction of wind-borne emissions and the associated dry-deposition field, while integrating exposed seabed soil salinity, vegetation cover and wind regimes. The contribution is the extension and aggregation of earlier regional models into a long-term, interval-based reconstruction that includes moderate wind conditions and paired vegetation scenarios.

# 2. Materials and methods

## Study Area Description

WST dynamics correspond to Aral Sea shrinking. The space under consideration was defined by 1961 Aral Sea coastline. This complex system, which includes shrinking water areas, increasing land areas after water disappearance and changing vegetation cover, was named Aral-61+. Long-term dynamics (1961-2025) of WST were studied.

The following processes mainly control WST parameters: Aral Sea desiccation, salinization of land areas after disappearing of water body, vegetation changes of land areas and rather constant wind regime. Thus, these processes' dynamics were considered within this study within the scope of study area.

The key driver of WST is the desiccation of the Aral Sea. This process (Fig. 2) can be divided into several stages. Figure 2.1 shows the Aral Sea as a unified body of water in 1964. In 1989, (Figure 2.2) the sea had separated into the Large Aral Sea in the south and Small Aral Sea in the north. In 2001 (Figure 2.3), the Large Aral Sea had separated into Western and Eastern basins. Figures 2.4-2.6 show periodic desiccation and partial refilling of the Eastern basin. From 2020 to 2024 (Figs. 2.7–2.8), no partial refilling occurred. The future trajectory of the Eastern basin may follow two scenarios: (a) complete and irreversible desiccation; or (b) continued periodic desiccation and partial refilling, provided there are water discharges from the Kokaral Dam, agricultural drainage system, and river inflow, alongside increased precipitation driven by global warming. For the Western basin of the Large Aral Sea, there are also two possible long-term trajectories: (a) complete and irreversible desiccation; or (b) stabilization if precipitation increases to match evaporation volumes.

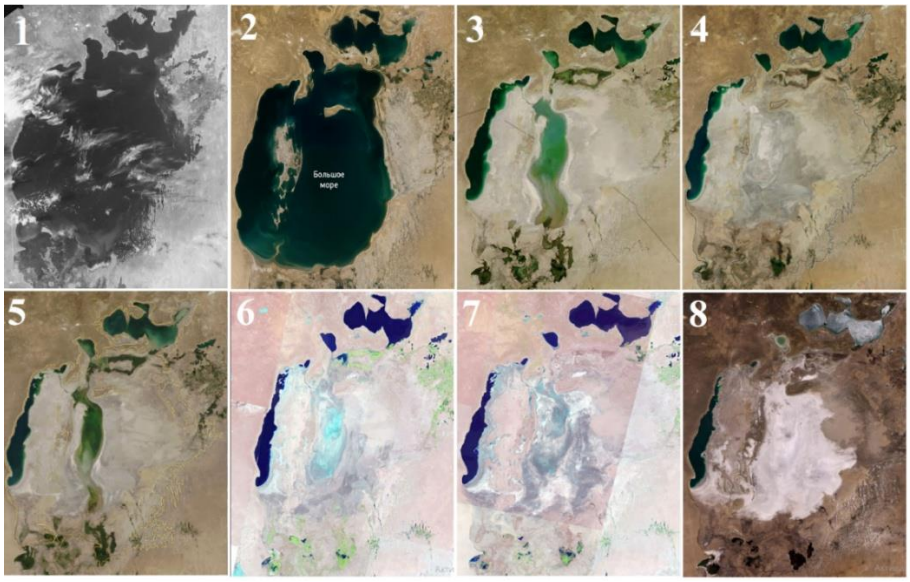


**Fig. 2**. Aral Sea dynamics during the study period (1961–2025). Historical satellite imagery; image provider, individual acquisition dates and reuse attribution require author confirmation.

Soil salinity on the exposed seabed, or post-aquatic land, is a driver of WST subordinate to the desiccation of the sea. Because the desiccation of the Aral Sea occurs predominantly during the warm season and is thus discontinuous, annual exposure bands are formed that differ in soil salinity and, consequently, in plant communities. These distinct differences are evidently driven by the year-on-year increase in water salinity.

The exposed seabed contains substantial salt reserves (Kurbaniyazov 2017; Letolle et al. 2005). The salt stock in the soil vadose zone has been reported to reach 2,200 t/ha (Orlovsky and Orlovsky 2001). Within the reported composition of Aral salt aerosol dust, sulfate salts account for 25–48%, chlorides for 18–30%, and carbonates for 10–20%. These fractions are not assumed to be uniform across the entire exposed seabed.

Vegetation cover (VC) is an important natural and managed factor regulating WST. Modeling studies (Kublanov and Tleumuratova 2023) indicate that vegetation attenuates wind speed and thereby reduces salt emission as a function of total projective cover (TPC). Vegetation may also indirectly influence WST through changes in soil properties and salinity. These mechanisms should be distinguished from the direct canopy

attenuation represented in the emission equations.

Plants on the shore expose to dynamic conditions depending on the soil salinity. Exposed areas develop zonations in the direction perpendicular to the shore, comparable to annual tree growth rings. The exposed areas become colonized by plant species in zonations with different salt tolerances. This makes the approach taken in this study to study long-term WST dynamics within exposure zones developed in different years suitable.

## Modeling Background

Long-range wind-blown salt transport, akin to a broad class of atmospheric pollution phenomena resulting from anthropogenic environmental impacts, is described by aerosol transport models in the lower atmosphere. Dust emission is governed by interactions between climate, soil properties (grain size, aggregation, structure, moisture and surface roughness), and vegetation (projective cover, distribution and height) across spatial and temporal scales (Shao et al. 2011a, 2011b; Zhang et al. 2011; Zobeck et al. 2000).

Physical dust models incorporate wind erosion, soil properties and atmospheric transport. Regional dust emission and transport schemes have been developed and applied with meteorological and climate datasets (Lu and Shao 2001; Zender et al. 2003; Barnum et al. 2004; LeGrand et al. 2019). Aerosol reanalysis and satellite observations, including aerosol optical depth, provide additional constraints on the distribution and prediction of dust (Randles et al. 2017; Benedetti et al. 2019).

Uncertainties exist within the modelled dust emissions, related to soil properties, emission parameters and meteorological data (Shao et al., 2011a, 2011b; LeGrand et al., 2019). Models developed for one region need to be validated and adjusted for application to different regions. The Aralkum is a drying sea bed that has highly variable surface properties and requires specific surface boundary conditions to represent the complex landscape pattern. Additionally, due to the increasing size of the region and changing salinity, the models previously developed for the Aral Sea are extended to include the time period 2005 – 2025.

## Modeling Approach

The Aral-61+ framework aggregates and interpolates earlier systemic numerical modeling results (Tleumuratova 2018; Kublanov 2023) into a regression-based reconstruction for 1961–2025. Its contribution is the explicit integration of successive exposure bands, time-varying salt availability, projective vegetation cover and wind regimes, with separate vegetation-adjusted and no-vegetation estimates and spatially distributed dry deposition. It extends the earlier MIDACS modeling approach beyond 2005 and includes moderate winds as well as storm conditions. It is a reduced-order regional reconstruction, not a newly calibrated atmospheric circulation or plant population model.

In many studies, the annual volume of dust emitted from the Aralkum is estimated by summing emissions during discrete dust storms occurring throughout the year. However, this approach overlooks quasi-stationary dust deflation under moderate wind speeds (5–10 m/s). A key distinction of the present work is the evaluation of WST parameters as a long-term exposure process, taking into account meteorological situations with moderate wind speeds. This approach contributed to a substantial increase in both the magnitude and spatial detail of the determined WST parameters. To isolate the contribution of dust storms to the annual salt export volume, separate calculations were conducted for wind speeds exceeding 10 m/s.

The simulation period (1961–2025) was divided into six complete ten-year intervals and a final five-year interval, 2021–2025. N = 1 represents 1961–1970, N = 2 represents 1971–1980, and N = 7 represents 2021–2025. The labels 1970, 1980, …, 2025 denote the corresponding interval endpoints, not necessarily single-year observations.

Furthermore, to account for interannual dynamics, time is identified both as the exposure time of a given calculation point on the exposed seabed (T = 1, 2, 3, . . . ), representing the number of years elapsed since the point emerged onto the surface, and as the desiccation time of the Aral Sea (t), measured in years starting from 1961. The modeling domain (Fig. 3) encompasses territories receiving ecologically significant levels of dry atmospheric deposition (DAD) of salts—i.e., zones of severe WST impact that increase soil salinity in adjacent areas by 0.13–0.18% annually (Tleumuratova 2018). Further expansion of the modeling domain would have reduced spatial detail and, consequently, the accuracy of the results.

**CONTACT** B.S. Tleumuratova

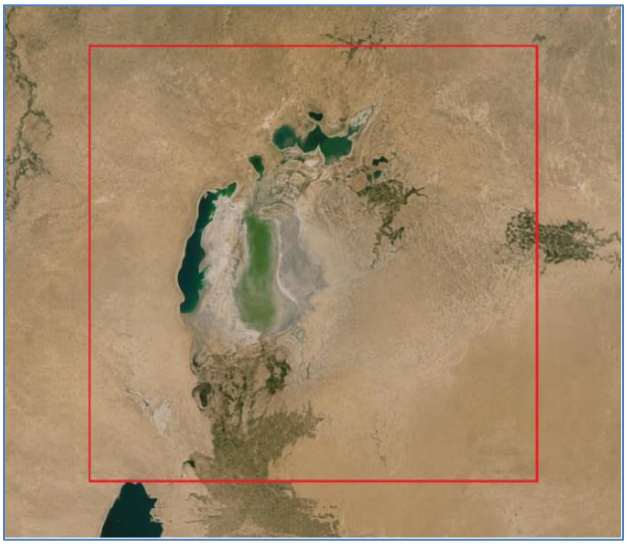

**Fig. 3.** Modeling domain. Boundary shown on a satellite basemap; original basemap provider, acquisition date and reuse attribution require author confirmation.

Spatial quantization corresponds to the temporal partitioning of the simulation period into decades: the exposed seabed is divided into exposure bands formed during 1961–1970, 1971–1980, etc. These exposure bands serve to identify the spatial distribution of soil salinity levels and the corresponding establishment of vegetation. It is assumed that soil salinization/desalinization processes and vegetation development progress along vectors normal to the shoreline of the respective year and remain approximately invariant along the entire length of each exposure band (Fig. 3). The orientation of the soil salinization vectors (white) and the corresponding decrease in total projective cover (green) are shown in Fig. 4 for the 2001–2010 exposure band.

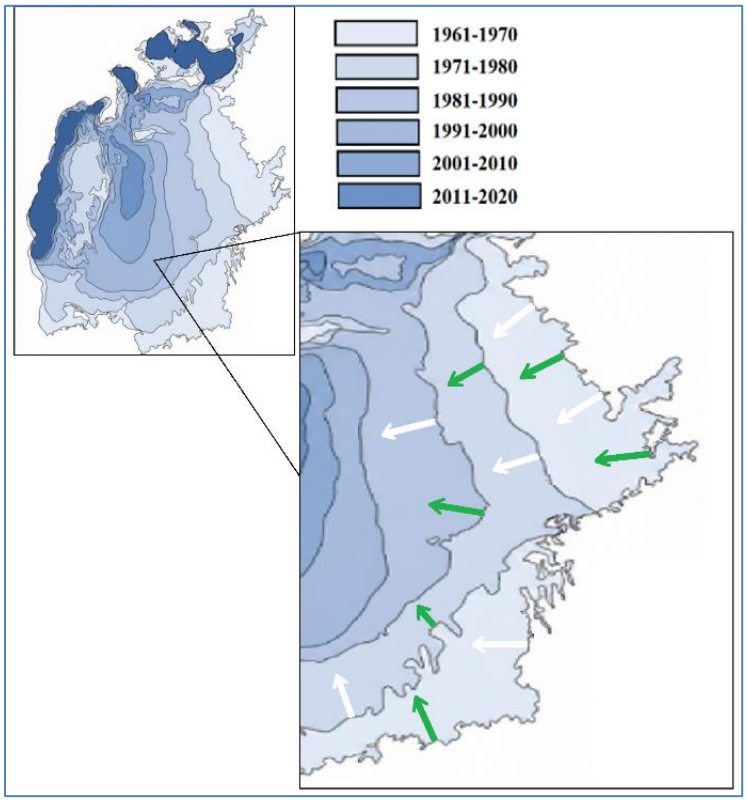


**Fig. 4.** Exposure bands of different decades from 1961 to 2020. Source: exposure-band schematic supplied with the Aral-61+ manuscript; underlying shoreline and basemap datasets require author confirmation.

The "Aral-61+" Model

The annual salt emission per unit area without vegetation is the product of source strength F and annual duration of energy-active wind speeds (>5 m/s), $T_e$ (hours/year), determined from meteorological handbooks (Tleumuratova 2002). Equation (1) requires compatible time and area units.

$$V_A = FT_e \qquad (Eq.1)$$

To determine source strength F (vertical flux of material per unit area per unit time), the formulation of Lu and Shao (2001) is applied:

$$F = \frac{0{,}12 C_{surf} g \rho_b}{p} aQ \qquad (Eq.2)$$

In Eq. (2), Q is horizontal salt mass flux (g $cm^{-1}$ $s^{-1}$), g is gravitational acceleration (9.81 m/$s^2$), ρb is the reported soil bulk density (2.6 g/$cm^3$), p is soil plastic pressure (0.5 MPa), Csurf is the surface salt concentration (Tleumuratova 2004), and a is salt content in the upper 0–20 cm soil layer. Csurf and a are mass fractions for dimensional consistency; their calibration convention and original numerical series must be confirmed. The value of ρb is retained as reported rather than assumed to be a measured local bulk density.

The representative particle density and diameter are 1.5 g/$cm^3$ and 10 μm, respectively; they are not explicit variables in Eq. (2). The horizontal flux Q is fixed at 0.159 g $cm^{-1}$ $s^{-1}$ (Semenov 2011). Its use across intervals is an approximation; sensitivity to Q is examined below.

The annual salt emission from the entire exposed Aral seabed (EAS) is therefore given by

$$V(N) = V_A S_{dr}(N) \qquad (Eq.3)$$

Here Sdr is the exposed seabed area for the corresponding interval. Equation (3) gives the no-vegetation emission estimate after conversion to tonnes/year.

The impact of vegetation cover (VC → WST) is represented by the reduction in source strength (ΔF) associated with wind attenuation within the canopy. The canopy wind profile relationship follows Bykova and Dubov (1974):

$$u_r = 0{,}83 \delta_f c_{Hh}^{0,5} u_a + (1 - \delta_f) u_a \qquad (Eq.4)$$

In Eq. (4), $u_a$ is background wind speed (m/s), $u_r$ is attenuated wind speed (m/s), and δf is the fraction of total projective vegetation cover. The reported regression δf = 87.918 exp(−0.114N) is in percent and must be divided by 100 when inserted as a fraction. The heat exchange coefficient c is reported as 0.023 W $m^{-1}$ $K^{-1}$. The source manuscript does not define Hh or its units in the canopy term; its original definition and normalization require confirmation from the underlying calculation. This prevents independent numerical reproduction of Eq. (4) from the manuscript alone.

The source-strength reduction is ΔF = F($u_a$) − F($u_r$). The corresponding annual reduction in emissions is given by Eq. (5), with TW denoting annual energy-active wind duration (the same quantity as $T_e$ in Eq. 1). Equation (2) does not explicitly specify Q as a function of wind speed; the wind-dependent flux calculation used to obtain F($u_a$) and F($u_r$) must be supplied to reproduce the vegetation-adjusted series independently.

$$V_{vc} = \Delta F T_W S_{dr} \qquad (Eq.5)$$

For agricultural zoning and human health risk assessment, identifying the spatial dynamics of the zone of influence is as critical as evaluating the multi-year dynamics of annual salt emission. In alignment with established methodologies, the impact of WST is quantified by the annual mass of salt deposited per unit area.

The areal salt emission source (Aralkum) is approximated as a collection of point sources distributed across exposure bands. This allows spatially varying band characteristics to be represented without assuming that the entire exposed seabed has a single emission strength. Each point source represents a contributing area, Sr; its annual emission is given by Eq. (6), with the same time and mass conversions as Eq. (1). For the vegetation-adjusted case F is evaluated using the attenuated wind conditions.

$$V_k = FT_W S_r \qquad (Eq.6)$$

Dry deposition of salt aerosol was calculated using the empirical relationship proposed in a previous study (Tleumuratova 2018), obtained by regression approximation of numerical simulations describing the long-term impact of wind-driven salt transport from the exposed Aral seabed:

$$C_{surf}(i,N) = 3{,}3 kV(N) \exp(-0{,}015x - 0{,}6)\, f_i(N) \qquad (Eq.7)$$

Here x is distance from a source (km) and $f_i$(N) is the frequency of the i-th wind direction for interval N. The exponential attenuation coefficient is 0.015 $km^{-1}$. The term kV(N) is interpreted as the annual emission associated with the individual point source; the precise mass-unit normalization and frequency convention for the fitted coefficient 3.3 must follow the original calibration (Tleumuratova 2018). The left-hand quantity in Eq. (7) represents the source-specific deposition field, rather than the surface soil salt concentration Csurf used in Eq. (2).

The dry-deposition field Cd for each point source is calculated in polar coordinates (distance and angle φ) for eight principal wind directions

and transformed to Cartesian coordinates (X, Y). The coordinate origin is at the lower-left corner of the modeling domain (Fig. 3), with X along the southern boundary and Y along the western boundary. Total dry salt deposition is obtained by summing the source-specific fields (Eq. 8).

$$C_d(S_{\text{oc}}) = \sum_{1}^{k} C_{dk}(X, Y) \qquad (Eq. 8)$$

## Data and Parameters

Literature sources, meteorological records (ASOS Mesonet and TerraClimate), and geospatial databases (Global Surface Water Explorer and USGS EarthExplorer) were used as inputs or comparison sources. These datasets were processed to match the interval-based spatial and temporal discretization. Table 1 presents the aggregated area, water salinity and vegetation indicators; Fig. 5 shows the wind-direction distributions. The final interval covers five years rather than ten.

Gypsum ($CaSO_4$) and mirabilite ($Na_2SO_4 \cdot 10H_2O$) are important sulfate components of Aral salt aerosol (Kurbaniyazov 2017). Atmospheric sulfate particles may occur in the submicron range (Milford and Davidson 1987), whereas larger carbonate and halite particles can settle more rapidly. The model uses a representative particle diameter of 10 μm, density of 1.5 t/m³ and dry deposition velocity of 5 mm/s (Zhang 2001 provides the background for size-dependent dry deposition). These are effective modeling assumptions, not measurements of a uniform Aralkum aerosol population. They do not resolve the size distribution or its spatial variation.

Available observational and literature inputs were aggregated by modeling interval to describe the spatiotemporal dynamics of the Aral Sea geosystem and exposed seabed (Table 1).

**Table 1.** Spatiotemporal dynamics of the "Aral-61+" geosystem components.

| Aral-61+ components | 1970 | 1980 | 1990 | 2000 | 2010 | 2020 | 2025 |
|---|---|---|---|---|---|---|---|
| Exposed seabed area (thousand km²) | 9.9 | 19.9 | 30.7 | 43.6 | 54.7 | 62.1 | 63.2 |
| Water Salinity in the Eastern and Western Parts | 14 | 18 | 32 | 92 | 220 | 350 | 356 |
| | 14 | 18 | 32 | 63 | 108 | 130 | 133 |
| Vegetation Cover Greater Than 20% (thousand km²) | 1.4 | 2.2 | 3.4 | 4.8 | 6.5 | 8.4 | 8.7 |
| Vegetation Cover Less Than 20% (thousand km²) | 3.7 | 8.4 | 9.4 | 11.2 | 13.1 | 16.7 | 16.8 |
| Area of Puffy Salt Marshes on Post-Aquatic Land (thousand km²) | 0.44 | 1.12 | 2.38 | 4.10 | 6.99 | 9.77 | 10.04 |

Note: Water salinity values are reproduced from the source table; the original manuscript does not specify their unit, which requires author confirmation. The vegetation-area categories are not equivalent to mean projective cover.

The wind regime of the study area was likewise statistically processed with decadal averaging. A rigorous statistical analysis of data from 1960 to 2025 recorded at the Muynak and Aralsk meteorological stations (Arushanov and Umerov 2026) revealed that the wind rose developed pronounced asymmetry across the entire simulation period, characterized by the suppression of all directions except north and northeast (Fig. 5).

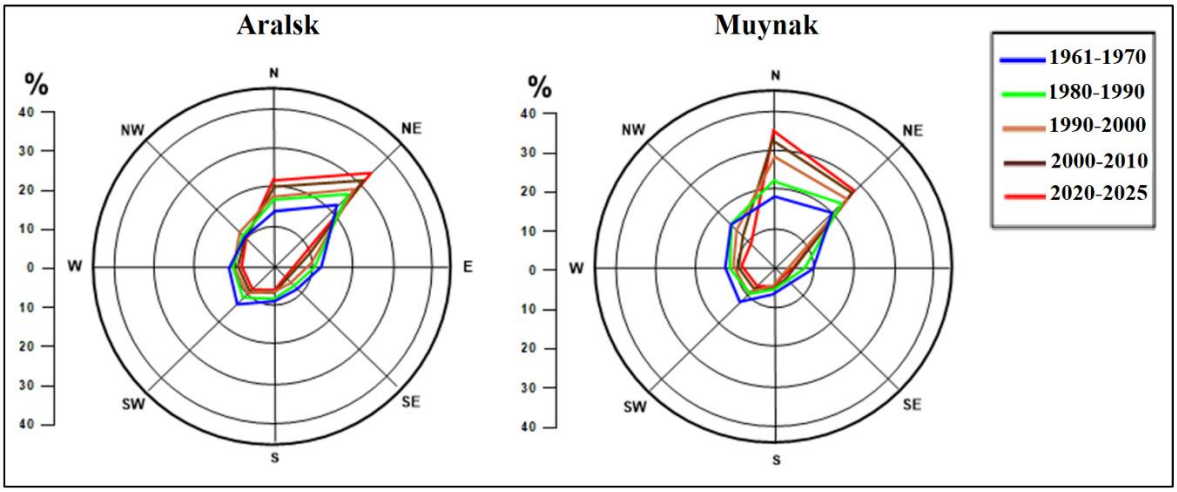


**Fig. 5.** Interval-averaged wind roses for the Aral Sea region. Source: manuscript analysis of Muynak and Aralsk meteorological station records (Arushanov and Umerov 2026, as cited in the original manuscript).

## Model implementation

## Computational workflow and discretization

Aral-61+ uses a time index N for the reporting interval and an exposure age T (years since emergence) for each band. The spatial domain is the 1961 shoreline and the surrounding deposition region shown in Fig. 3. For each interval, the exposed seabed is partitioned into newly exposed and previously exposed bands, with approximately uniform conditions along each band and variation normal to the shoreline (Fig. 4). The point-source approximation represents each band by a set of uniformly distributed sources. Let $A_n$ be the area of band n (m²), $K_n$ the number of representative sources and $A_{nk}$ the area represented by source k, so that $\Sigma_k A_{nk} = A_n$. The spatial representation must conserve band area.

1. Aggregate the available shoreline, salinity, vegetation and wind records for each interval, using annualized wind durations for the final five-year period. Assign surface salt concentration and upper-soil salt content to each exposed band as functions of exposure age and the associated regression inputs. Table 1 records the aggregate indicators; the original band-level regression coefficients and input arrays are not included in the manuscript.

2. Calculate the reference emission flux F using Eq. (2). Evaluate Eq. (1) for winds above 5 m/s and separately for winds above 10 m/s to estimate the storm contribution. If F is expressed in g $cm^{-2}$ $s^{-1}$, convert to kg $m^{-2}$ $s^{-1}$ by multiplying by 10; multiply the annual duration in hours by 3,600 and the represented area in m², and divide kilograms by 1,000 to obtain tonnes/year. Use the same unit convention throughout.

3. Evaluate vegetation attenuation using Eq. (4), then the reduction in source strength and annual emission from Eq. (5). The vegetation-adjusted interval emission is $Vveg = V_0 - \Delta V$, where $V_0$ is Eq. (3) and $\Delta V$ is Eq. (5). The original chart data provide the paired estimates plotted in Fig. 6.

4. Calculate source emission using Eq. (6), conserving the area-weighted total across all bands. For each source and receptor, compute distance in kilometers and assign the appropriate downwind sector from the eight-direction wind rose. Wind directions reported meteorologically are directions of origin; the corresponding transport direction is opposite. Evaluate the empirical deposition kernel in Eq. (7), and sum contributions using Eq. (8) to obtain a field in kg/ha/year, as reported in Fig. 7.

5. Extract the annual dry-deposition contours and compare their spatial extent. A reproducible influence-area calculation would sum the areas of receptor cells exceeding a specified threshold, e.g., 20 kg/ha/year; here only the reported directional contour distances are interpreted because the receptor grid and contour polygons are unavailable.

## Reproducibility requirements

The framework above defines the mathematical sequence supported by the supplied manuscript, but exact reconstruction of Tables 1–2 and Fig. 7 additionally requires the original regression coefficient tables, band-level Csurf and a values, annual wind durations and wind-dependent Q relationship, canopy parameter Hh, point-source coordinates and weights, receptor-grid spacing and coordinate reference system, and the calibration units of Eq. (7). These were not reported in the original text. The tabulated outputs are retained rather than regenerated from assumed inputs. The authors should make the original implementation and preprocessing inputs available with these metadata.

## Mathematical link to vegetation dynamics

Let S n (T) be salinity (%) in band n of exposure age T and P n (T) be the total projected cover in band n (unitless). The model considers these as temporally varying covariates. On aggregation, this reduces to P (N)= 0.87918e -0.114N, so dP/dN = -0.114P. This is a model for the reduction in projected cover as exposure ages, but is not specific to any species. The causal relationships for this process at source resolution are S n(T) → P n(T) → u r → F → V veg. Under salt limited succession, increased salinity may reduce P. This results in reduced canopy shading and higher salt emissions. Previously exposed bands may have different responses to changing salinities.

The canopy component (Eq. 4) can be expressed as u r = u a (1 - P(1-B)). Here, B is dimensionless. B is multiplied by P in the initial term of the equation. As described in the equation, B includes the coefficient (0.83) and expression for canopy parameters. Holding B and u a constant, the partial derivative of u r with respect to P is $\partial u_r / \partial P = u_a (B-1)$. Thus when the canopy is reducing ($B < 1$), this derivative is negative. Assuming that the wind dependent salt emission flux increases with increasing wind speed, $\partial F/\partial P = (\partial F/\partial u_r) u_a (B-1) \leq 0$. This represents a causal relationship between projected cover and salt emission. However, it does not mean that the model predicts species abundance, germination rates or fits a function describing the effect of salinity on vegetation. Instead, a function would require independent ecological observations.

## 3. Results and Discussion

Table 2 summarizes the modeled state of the exposed seabed for the seven intervals. The annual salt emission row corresponds to the vegetation-adjusted series in Fig. 6; the no-vegetation series is presented separately in that figure.

**Table 2.** Summary parameters of the Aral Sea geosystem and its exposed seabed.

| | Unit | | Interval endpoint | | | | | | |
|---|---|---|---|---|---|---|---|---|---|
| | | | 1970 | 1980 | 1990 | 2000 | 2010 | 2020 | 2025 |
| Average Soil Salinity | % | | 0.65 | 2.2 | 4.4 | 7.6 | 13.9 | 20.9 | 21.5 |
| TPC (regional) | East | % | 74.1 | 67.2 | 63.1 | 49.7 | 42.7 | 38.1 | 37.4 |
| | West | % | 80.1 | 71.6 | 67.8 | 62.7 | 53.6 | 51.1 | 49.8 |
| Salt emissions (with vegetation) | million tonnes/year | | 0.7 | 12.6 | 41.1 | 65.8 | 107.4 | 128.4 | 131.5 |

Note: TPC = total projective cover; East and West denote the reported regional indicators. The 2025 endpoint covers 2021–2025. Values are retained from the original table and chart.

The annual salt emission estimates in Table 2 and Fig. 6 increase monotonically but not at a constant or continuously accelerating rate. The vegetation-adjusted series rises from 0.7 million tonnes/year at the 1970 endpoint to 107.4 in 2010, 128.4 in 2020 and 131.5 in 2025. The increase between the 2000 and 2010 endpoints is 41.6 million tonnes/year, compared with 21.0 between 2010 and 2020 and 3.1 between 2020 and 2025. Dividing by elapsed endpoint years gives 4.16, 2.10 and 0.62 million tonnes/year per year, respectively. The recent slowdown is consistent with the reduced expansion of exposed land (Table 1).

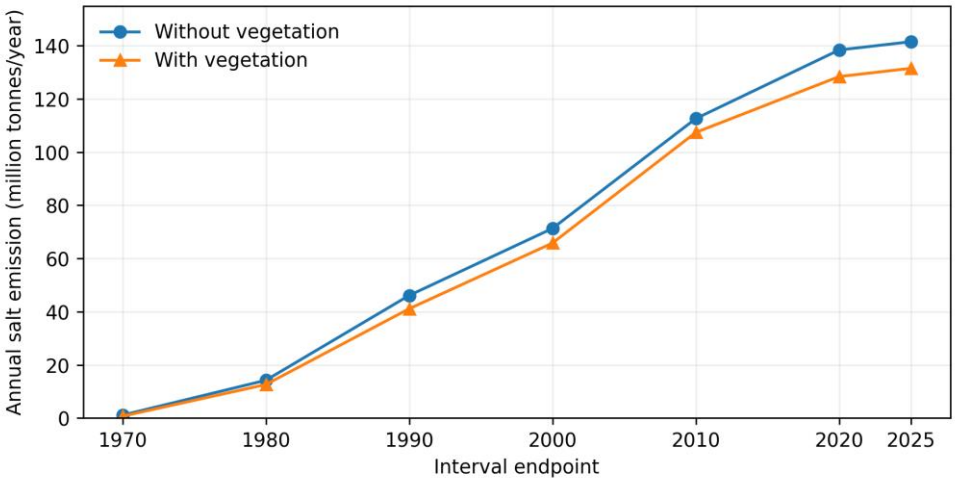


**Fig. 6.** Annual salt emission from the exposed seabed, with and without vegetation cover, by interval endpoint. Source: original Aral-61+ chart series (replotted from the embedded numerical data); lines connect interval estimates and are not predictions between endpoints.

Nonlinearity reflects the interacting changes in exposure area, water salinity, exposed soil salinity and vegetation TPC (Tleumuratova 2018; Kublanov 2023). The original no-vegetation estimates for 2020 and 2025 are 138.4 and 141.5 million tonnes/year, respectively, compared with 128.4 and 131.5 with vegetation. The corresponding relative reductions are 7.2% and 7.1%, calculated as $100 \times (V_0 - Vveg)/V_0$. These estimates describe the model's paired scenarios, not an independently measured effect of afforestation.

Comparisons between emission estimates from literature and model time series are limited. However, emission estimates from literature (43 Mt year -1) can be compared to those at the end of the period (1990, 41.1 Mt year -1 ), resulting in a relative error of -4.4% [(modelling estimate - literature estimate)/literature estimate 100]. Comparisons cannot be made to exactly the same date. Emission estimates from literature in 2000 show higher values: 53 Mt year -1 and 57 Mt year -1 from the surface and drying zones respectively, and 13 Mt year -1 from salinized soils (Chub 2000). Total emissions (123 Mt year -1) include emissions from surface water so comparisons to emissions from exposed seabed in this model are not appropriate. Assuming that the drying zone and salinized soil sources are separate, total emissions would be 70 Mt year -1. The modelled value for 2000 is 65.8 Mt year -1 resulting in a relative error of -6.0%. Therefore this comparison does not validate predictive capability. To formally validate, salt only emission data from equivalent regions and periods would need to be found.

Increases in dust storms have been observed in this region (Wang et al. 2022, Indoitu et al. 2015, Shi et al. 2020). This supports the general increasing trend in salt emissions in the model, however does not quantify the magnitude of increases or challenge the recent decreasing trend. On average, 60% of total annual WST originates from wind speeds > 10ms -1 in the period studied. This is a model derived figure and not validated.

## The extent of WST over multiple years

The extent of WST in multiple years was determined from annual dry salt deposition in this model (Kublanov 2023, Indoitu et al. 2015, Goudie 2014, Shi et al. 2020, Tleumuratova 2018). Variations exist in the estimates given in different studies due to differences in method, period, source origin and coverage.

Annual dry salt deposition for 1990 and 2024 are shown in Fig. 7. The highest values in both years occur around Kungrad and Muynak, to the south west of the Aralkum. The 20 kg ha -1 contour extended 150 km to the south and 500 km to the south west in 1990, compared to 300km to the south and 800km to the south west in 2024. This suggests that the extent of WST in the model has increased. However, without calculating the total area covered by each contour polygon, it is impossible to determine the total area of WST, or rate of linear increase in area.

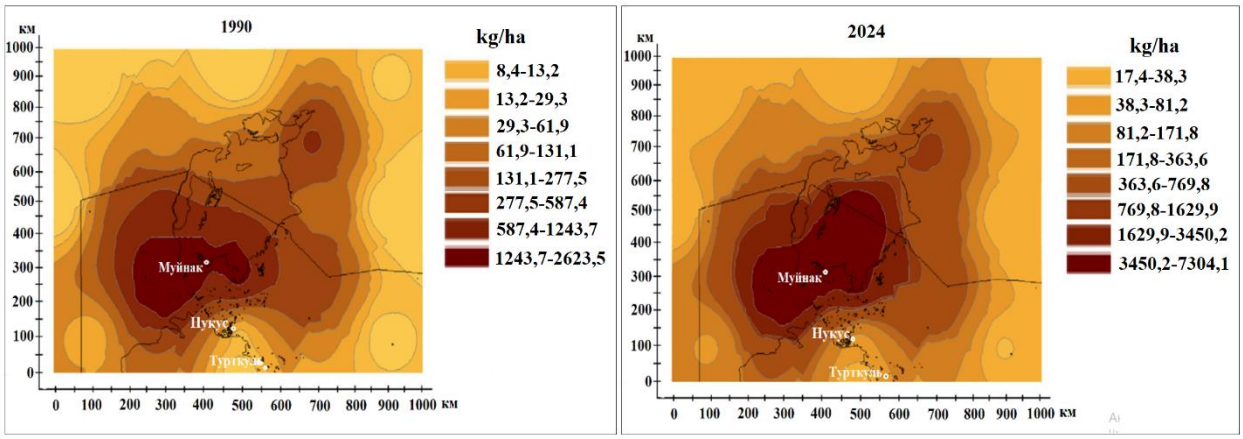


**Fig. 7**. Modeled annual mean dry salt deposition (kg/ha) in 1990 and 2024. Source: Aral-61+ manuscript simulation outputs; underlying basemap provenance requires author confirmation.

Only sparse comparisons are possible for the modeled zone of influence. Using a hydrodynamic storm model, Kaipov (1995) and Semenov et al. (1990) reported salt-and-dust deposition in the Amu Darya delta of 1.5–6.0 t/ha, including 170–800 kg/ha of soluble salts and up to 1,800 kg/ha on the exposed seabed. Differences between the two methods ranged from 5.4 to 10.2 times higher. However, since exact matching sites, time periods and specific deposition rates by source are unknown, these differences cannot be considered to be repeatable error margins. Furthermore, it is uncertain whether the storm calculation represents the same amount as only dry salt deposition annually.

In irrigated Karakalpakstan, dry deposition of salts was between 150 and 300 kg/ha, but soluble salt accounted for only 2-30% of total salts (Razakov and Kosnazarov, 1998). Differences in this study were between 2.3 to 4.9 times. As there was no matching information on the proportion of soluble salt at each site, and length of time period averaged over, this information cannot be used to quantify any bias in the model. Differences in the total dust and soluble salts, other sources contributing to deposition and spatial heterogeneity may be responsible for these differences.

Wet deposition. Salt deposition via precipitation was between 150 and 300 kg/ha per year (Razakov and Kosnazarov, 1998). Salinity in precipitation increased from 30-100 mg/L pre-1975 to 100-150 mg/L in later observations. . These values illustrate that wet scavenging may be substantial, but cannot simply be added to modeled dry deposition because precipitation affects the airborne salt reservoir and the spatial and temporal partitioning of deposition. The modeled contours must therefore be interpreted as dry deposition only, rather than total ecosystem salt loading.

The monotonic distance-decay kernel in Eq. (7) is a simplification that may represent relatively coarse particles more adequately than fine aerosols. Finer particles can remain suspended and produce secondary deposition or concentration maxima (Tolkacheva 2000; Tleumuratova 2004, 2018; Banks et al. 2022). The radial one-dimensional kernel, combined across sources and directions to form a two-dimensional field, does not explicitly resolve size-dependent atmospheric transport, vertical mixing or secondary maxima. Consequently, the modeled contours may miss distant exposure hotspots. Independent size-resolved transport and deposition observations would be necessary to evaluate this structural uncertainty.

## Analytical sensitivity and uncertainty

A local one-at-a-time sensitivity analysis was conducted directly from the reported emission and deposition equations, holding all other quantities and the canopy correction fixed. From Eqs. (1)–(3), the reference annual emission is proportional to Csurf, ρb, a, Q, $T_e$ and Sdr and inversely proportional to p. For a parameter z, the normalized elasticity is $E_z = (z/V_0)(\partial V_0/\partial z)$. Thus the elasticities for the direct factors are +1 and that for p is −1. These are structural sensitivities, not uncertainty distributions or reruns of the coupled model.

For Eq. (7), write $D(x) = A \exp(-\beta x - 0.6)$ with $\beta = 0.015$ km$^{-1}$ and A representing the fixed source and directional factors. The relative response to a perturbation Δβ is $D'/D = \exp(-x\Delta\beta)$. The elasticity with respect to β is −βx. Increasing β by 10% causes the kernel to decrease by 13.9% (100km) and 25.9% (200km). Decreasing β by 10% causes an increase of the kernel by 16.2% (100km) and 35.0% (200km). Sensitivity increases with distance, which indicates that the limits for the deposition zone are highly dependent on the assumed attenuation parameter.

Table 3. Local analytical sensitivity of the reported emission and deposition equations to illustrative ±10% perturbations.

| Parameter / output | −10% | +10% | Elasticity |
|---|---|---|---|
| Csurf, ρb, a, Q, $T_e$ or Sdr / $V_0$ | −10.0% | +10.0% | +1 |
| p / $V_0$ | +11.1% | −9.1% | −1 |

| | | | |
|---|---|---|---|
| β / D at 100 km | +16.2% | −13.9% | −1.5 |
| β / D at 200 km | +35.0% | −25.9% | −3.0 |

The results from varying the no vegetation rate in 2025 by +/-10% (Q) gives values between 127.35-155.65Mtonnes per year. It should be noted that this variation of the results within these bounds does not represent additional model runs or error margins. As particle diameter, density and dry deposition velocities are not explicit in the regression kernel provided, it is impossible to identify individual effects within these equations. Interactions between different parameters, uncertainty in calibrating the canopy, and exclusion of wet deposition and multimodal transport mean further numerical investigation is required. Finally, this +/-10% variation has been chosen arbitrarily rather than being an estimated parameter range.

Future trends in WST will largely depend on what trend occurs within the Eastern basin and how climate change progresses. (Fig 8).

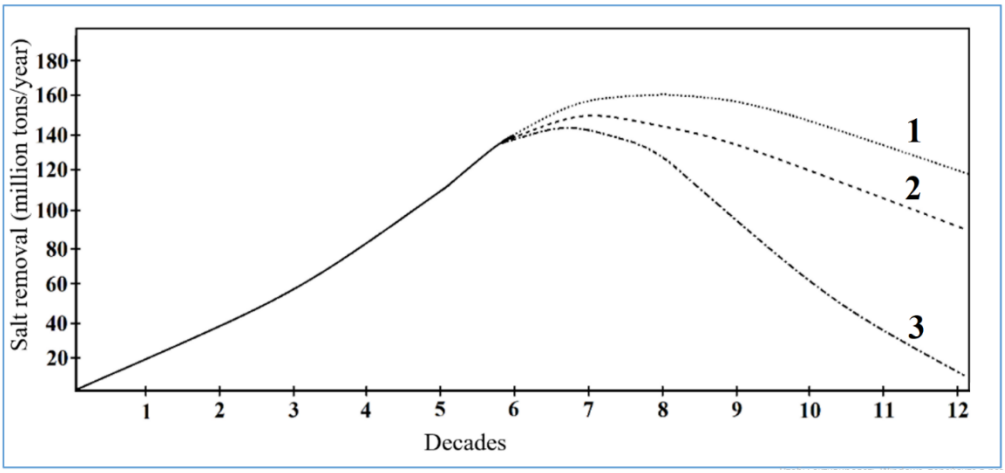


**Fig. 8**. Conceptual scenarios for future WST dynamics (not calibrated forecasts). Source: scenario schematic supplied with the original manuscript.

Scenario 1: If the Eastern Basin is completely dried out with large areas of solonchak formation, increased summer temperatures and reduced rainfall, then annual emissions may increase. However, this high emission rate (171.4 million tonnes per year between 2030 and 2040) is based upon an initial conceptual model and therefore cannot be taken as a confirmation. The assumptions made to determine this, alongside the method itself, must be considered separately. Eventually salt resources within the system may become limited, reducing emissions.

Scenario 2: If managed outflows are maintained, with rainfall levels sufficient to maintain the Eastern Basin in a similar state to 2010-2020, then further exposure of saline land may be limited. In these conditions, WST may stabilise by 2030-2040 before decreasing. However, it is uncertain how quickly and how much WST will decrease.

Scenario 3: This scenario is hypothetical. Meteorological feasibility; water availability, soil wetting, salt dissolution, wet deposition and ecological effects must be considered. A reduction of up to 80% as presented in this scenario is illustrative only. It does not represent either a calculated or observed reduction caused by Aral-61+. If a reduction of 0.8 was applied to the 2025 vegetation adjusted baseline (of 131.5 million tonnes per year), then 26.3 million tonnes per year would be emitted. However, this example does not prove that increasing precipitation leads to this level of reduction, nor a reduction in total deposition.

In scenarios 2 and 3, reductions in emissions may depend upon when and for how long mitigation measures are applied. If mitigation is stopped, emissions may increase again, as salts may be available for emission. In order to quantify this effect, it is necessary to model salt mass balance alongside precipitation, soil moisture and emission.

Earlier modeling (Kublanov and Tleumuratova 2023) estimated a potential 15–20% reduction under its own phytoremediation assumptions. That estimate should not be conflated with the present paired scenarios, which show a 7.1% reduction at the 2025 endpoint. Although the area with vegetation cover exceeding 20% grows from 1.4 to 8.7 thousand km² (Table 1), the corresponding exposed area also grows from 9.9 to 63.2 thousand km². The two regional TPC indicators decline (Table 2). Increasing planted area therefore does not imply increasing mean cover or proportional emission control. Establishment and persistence of vegetation depend on local soil salinity, moisture and species tolerance, none of which are independently resolved as population dynamics in the present regression framework.

## 4. Conclusion

Negative anthropogenic impacts on the natural environment have generated a multitude of climatological and ecological problems. In particular, a broad spectrum of environmental pollution issues is characterized by a critical feature: unpredictability. Consequently, there is an urgent need to investigate these processes in conjunction with their underlying drivers and affected targets to identify evolutionary trends and improve forecasting accuracy. This study addressed the practically significant task of reconstructing the multi-year dynamics of WST over the 1961–2025

period. With appropriate adaptation to regional geographic conditions, the obtained results can be applied to the diagnosis and forecasting of saline lake desiccation,a phenomenon occurring across many regions globally due to climate change.

The systems analysis and reduced-order regression framework reconstruct the monotonic, nonlinear increase in annual salt emissions while accounting for exposed seabed salinity and vegetation cover. The vegetation-adjusted estimate increases from 0.7 million tonnes/year at the 1970 endpoint to 131.5 at the 2025 endpoint. The endpoint-to-endpoint mean rate of change is (131.5 − 0.7)/55 = 2.38 million tonnes/year per year, not an average computed from annual observations across 1961–2025. Growth slows substantially in the latest interval, and the paired no-vegetation and vegetation scenarios indicate a 7.1% reduction in 2025.

The future WST depends on solonchak extent, wind regimes, soil moisture and mitigation. Salt land exposure may increase in the future, meaning that WST could continue to increase. However wind and precipitation patterns require further investigation. Phytoremediation is important in reducing WST, but effectiveness will depend on local salinity levels and establishment conditions. Artificial precipitation enhancement is tentative, so feasibility and effectiveness can not be confirmed. The results of the Aral-61+ case study give an approximate framework to compare deposition between regions, however are not a fully validated prediction. Further studies should aim to match field measurements, include size resolved transport, wet deposition, specific plant succession, and full transparency in numerical inputs and calibrations.

## References

Arushanov M. L and Umerov H. U. 2026. *Evaluation of the Classical and Modified Ginu Functions in Relation to the Aralkum Desert Conditions*. May 7. https://doi.org/10.5281/ZENODO.20067964.

Azydova, R. N., and O. E. Semenov. 1985. 'Assessment of Wind Sand Transport Volumes in the Aral Sea Region Based on Meteorological Station Observations'. In *Proceedings of Kazakh Research Institute of Hydrometeorology*, 85. C.

Banks, Jamie R., Bernd Heinold, and Kerstin Schepanski. 2022. 'Impacts of the Desiccation of the Aral Sea on the Central Asian Dust Life-Cycle'. *Journal of Geophysical Research: Atmospheres* 127 (21): e2022JD036618. https://doi.org/10.1029/2022JD036618.

Barnum, B., N. Winstead, J. Wesely, et al. 2004. 'Forecasting Dust Storms Using the CARMA-Dust Model and MM5 Weather Data'. *Environmental Modelling & Software* 19 (2): 129–40. https://doi.org/10.1016/S1364-8152(03)00115-4.

Benedetti, Angela, Francesca Di Giuseppe, Luke Jones, Vincent-Henri Peuch, Samuel Rémy, and Xiaoye Zhang. 2019. 'The Value of Satellite Observations in the Analysis and Short-Range Prediction of Asian Dust'. *Atmospheric Chemistry and Physics* 19 (2): 987–98. https://doi.org/10.5194/acp-19-987-2019.

Bykova, D. P., and A. S. Dubov. 1974. 'The Influence of Forest Shelterbelts on the Distribution of Dust Concentration during Dust Storms'. *Meteorology and Hydrology*, no. 7: 23–36.

Chub, V. E. 2000. *Climate Change and Its Impact on the Natural Resource Potential of the Republic of Uzbekistan*. (Tashkent, Uzbekistan), 252.

Ge, Yongxiao, Na Wu, Jilili Abuduwaili, Rashid Kulmatov, Gulnura Issanova, and Galymzhan Saparov. 2022. 'Identifying Seasonal and Diurnal Variations and the Most Frequently Impacted Zone of Aerosols in the Aral Sea Region'. *International Journal of Environmental Research and Public Health* 19 (21): 14144. https://doi.org/10.3390/ijerph192114144.

Goudie, Andrew S. 2014. 'Desert Dust and Human Health Disorders'. *Environment International* 63 (February): 101–13. https://doi.org/10.1016/j.envint.2013.10.011.

Goudie, A.S., and N. J. Middleton. 2006. *Desert Dust in the Global System*. Springer.

Indoitu, R., G. Kozhoridze, M. Batyrbaeva, et al. 2015. 'Dust Emission and Environmental Changes in the Dried Bottom of the Aral Sea'. *Aeolian Research* 17 (June): 101–15. https://doi.org/10.1016/j.aeolia.2015.02.004.

Kaipov, I. V. 1995. 'Modeling of Wind-Sand Flow Transformation under Changes in Surface Characteristics'. In *Current Problems of Hydrometeorology of Lake Balkhash and the Balkhash Region*. Saint Petersburg.

Kosnazarov, K. A. 2005. 'Impact of Aeolian Transport of Salt and Dust on Abiotic Components in the Southern Aral Sea Region'. *Study of Environmental Problems of the Aral Sea Region: Proceedings of the Scientific and Practical Conference* (Nukus, Uzbekistan).

Kublanov, Zh. Zh. 2023. 'Quantitative Assessment of the Salt Parameter Dynamics of the Desiccated Aral Sea Bed'. PhD dissertation, Karakalpak Scientific Research Institute of Natural Sciences. Originally published as *Количественная оценка солевого параметра динамики осушенного дна Аральского моря*.

Kublanov, Zh. Zh., and B. S. Tleumuratova. 2023. 'Assessment of the Effectiveness of Anthropogenic Impacts on Salt Emission Reduction from the Desiccated Aral Sea Bed'. *Universum: Chemistry and Biology* 2 (104): 15–21. Originally published as *Оценка эффективности антропогенных воздействий на осушенном дне Аральского моря по ослаблению выноса солей*.

Kurbaniyazov, A. K. 2017. *Evolution of Landscapes of the Exposed Aral Sea Bed*. Publishing House of the Academy of Natural Sciences. Moscow.

LeGrand, Sandra L., Chris Polashenski, Theodore W. Letcher, Glenn A. Creighton, Steven E. Peckham, and Jeffrey D. Cetola. 2019. 'The AFWA Dust Emission Scheme for the GOCART Aerosol Model in WRF-Chem v3.8.1'. *Geoscientific Model Development* 12 (1): 131–66. https://doi.org/10.5194/gmd-12-131-2019.

Letolle, Rene, Nicholas Aladin, Igor Filipov, and N. G. O. Boroffka. 2005. 'The Future Chemical Evolution of the Aral Sea from 2000 to the Years 2050'. *Mitigation and Adaptation Strategies for Global Change* 10 (1): 51–70. https://doi.org/10.1007/s11027-005-7830-2.

Li, Yizhen, Long Ma, Yongxiao Ge, and Jilili Abuduwaili. 2022. 'Health Risk of Heavy Metal Exposure from Dustfall and Source Apportionment with the PCA-MLR Model: A Case Study in the Ebinur Lake Basin, China'. *Atmospheric Environment* 272 (March): 118950. https://doi.org/10.1016/j.atmosenv.2022.118950.

Lu, Hua, and Yaping Shao. 2001. 'Toward Quantitative Prediction of Dust Storms: An Integrated Wind Erosion Modelling System and Its Applications'. *Environmental Modelling & Software* 16 (3): 233–49. https://doi.org/10.1016/S1364-8152(00)00083-9.

Máté, Bartus, Károly Barta, Jozsef Szatmari, and Andrea Farsang. 2017. 'Modeling Wind Erosion Hazard Control Efficiency with an Emphasis on Shelterbelt System and Plot Size Planning'. *Zeitschrift Für Geomorphologie* 61 (August). https://doi.org/10.1127/zfg/2017/0406.

Micklin, Philip. 2004. 'The Aral Sea Crisis'. In *Dying and Dead Seas Climatic Versus Anthropic Causes*, edited by Jacques C. J. Nihoul, Peter O. Zavialov, and Philip P. Micklin. Springer Netherlands. https://doi.org/10.1007/978-94-007-0967-6_5.

Micklin, Philip. 2007. 'The Aral Sea Disaster'. *Annual Review of Earth and Planetary Sciences* 35 (Volume 35, 2007): 47–72. https://doi.org/10.1146/annurev.earth.35.031306.140120.

Micklin, Philip P. 1988. 'Desiccation of the Aral Sea: A Water Management Disaster in the Soviet Union'. *Science* 241 (4870): 1170–76. https://doi.org/10.1126/science.241.4870.1170.

Milford, Jana B., and Cliff I. Davidson. 1987. 'The Sizes of Particulate Sulfate and Nitrate in the Atmosphere—A Review'. JAPCA 37 (2): 125–34. https://doi.org/10.1080/08940630.1987.10466206.

Mozhaitseva, N. F., and T. F. Nekrasova. 1984. 'Method for Estimating Wind-Borne Salt Removal from the Exposed Aral Sea Bed'. *Problems of Desert Development*, 15–21.

Nobakht, Mohamad, Maria Shahgedanova, and Kevin White. 2021. 'New Inventory of Dust Emission Sources in Central Asia and Northwestern China Derived From MODIS Imagery Using Dust Enhancement Technique'. *Journal of Geophysical Research: Atmospheres* 126 (4): e2020JD033382. https://doi.org/10.1029/2020JD033382.

Novitskiy, Z. B., A. H. Hamzayev, N. Zh Bakirov, and G. H. Atadjanova. 2024. 'Aral Environmental Disaster and Its Mitigation Through Forest Plantations'. *IOP Conference Series: Earth and Environmental Science* 1405 (1): 012026. https://iopscience.iop.org/article/10.1088/1755-1315/1405/1/012026/meta.

Orlovsky, L., and N. Orlovsky. 2001. *White Sand Storms in Central Asia*. UNCCD report,. Edited by Y. Youlin, V. Squired, and L. Qi. Bangkok.

Parajuli, Sagar P., and Charles S. Zender. 2018. 'Projected Changes in Dust Emissions and Regional Air Quality Due to the Shrinking Salton Sea'. *Aeolian Research* 33 (August): 82–92. https://doi.org/10.1016/j.aeolia.2018.05.004.

Pope, C. Arden, III. 2002. 'Lung Cancer, Cardiopulmonary Mortality, and Long-Term Exposure to Fine Particulate Air Pollution'. JAMA 287 (9): 1132. https://doi.org/10.1001/jama.287.9.1132.

Randles, C. A., A. M. Da Silva, V. Buchard, et al. 2017. 'The MERRA-2 Aerosol Reanalysis, 1980 Onward. Part I: System Description and Data Assimilation Evaluation'. *Journal of Climate* 30 (17): 6823–50. https://doi.org/10.1175/JCLI-D-16-0609.1.

Razakov, R. M., and K. A. Kosnazarov. 1987. 'Aeolian Transport and Deposition of Salt-Dust Particles in the Aral Sea Region'. In *Problems of the Aral Sea and Environmental Protection Measures*. Tashkent, Uzbekistan.

Razakov, R. M., and K. A. Kosnazarov. 1998. 'Migration of Salts and Toxicants in the Aral Sea Region. Problems of Desert Development'. *Problems of Desert Development*, nos 3–4: 63–70.

Rubanov, I. V., and N. M. Bogdanova. 1987. 'Quantitative Assessment of Salt Deflation from the Drying Bed of the Aral Sea'. *Problems of Desert Development*, no. 3: 9–16.

Semenov, O. E. 2011. 'Particle Velocity and Sand Mass Flux Profile in the Boundary Layer of Wind-Sand Flow'. *Hydrometeorology and Ecology*, no. 3: 30–49.

Semenov, O. E., I. V. Kaipov, and A. P. Shapov. 1990. 'Sand-Salt Storms in the Aral Sea Region'. In *Hydrometeorological Problems of the Aral Sea Region*, Gidrometeoizdat. Leningrad.

Shao, Y., M. Ishizuka, M. Mikami, and J. F. Leys. 2011a. 'Parameterization of Size-Resolved Dust Emission and Validation with Measurements'. Journal of Geophysical Research 116 (D8): D08203. https://doi.org/10.1029/2010JD014527.

Shao, Yaping, Karl-Heinz Wyrwoll, Adrian Chappell, et al. 2011b. 'Dust Cycle: An Emerging Core Theme in Earth System Science'. Aeolian Research 2 (4): 181–204. https://doi.org/10.1016/j.aeolia.2011.02.001.

Shi, Lamei, Jiahua Zhang, Fengmei Yao, Da Zhang, and Huadong Guo. 2020. 'Temporal Variation of Dust Emissions in Dust Sources over Central Asia in Recent Decades and the Climate Linkages'. *Atmospheric Environment* 222 (February): 117176. https://doi.org/10.1016/j.atmosenv.2019.117176.

Singer, A., T. Zobeck, L. Poberezsky, and E. Argaman. 2003. 'The PM10and PM2·5 Dust Generation Potential of Soils/Sediments in the Southern Aral Sea Basin, Uzbekistan'. *Journal of Arid Environments* 54 (4): 705–28. https://doi.org/10.1006/jare.2002.1084.

Skiles, S. McKenzie, Mark Flanner, Joseph M. Cook, Marie Dumont, and Thomas H. Painter. 2018. 'Radiative Forcing by Light-Absorbing Particles in Snow'. *Nature Climate Change* 8 (11): 964–71. https://doi.org/10.1038/s41558-018-0296-5.

Tleumuratova, B. S. 2002. 'Mathematical Modeling of Salt Transport from the Desiccated Aral Sea Bed during Dust Storms'. *Obyedinennyi Nauchnyi Zhurnal*, 28 51-40-42.

Tleumuratova, B. S. 2004. 'Mathematical Modeling of Aerosol Transport in the Lower Atmospheric Layers'. Doctoral dissertation, Tashkent, Uzbekistan.

Tleumuratova, B. S. 2009. 'Influence of Salt-Dust Transport on Sedimentation Processes in the Aral Sea Region'. *Arid Ecosystems*, no. 3(39): 15.

Tleumuratova, B. S. 2018. 'Mathematical Modeling of the Influence of Ecosystem Transformations in the Southern Aral Sea Region on Soil and Climatic Conditions'. Doctoral dissertation, National University of Uzbekistan. Originally published as *Математическое моделирование влияния трансформаций экосистемы Южного Приаралья на почвенно-климатические условия*.

Tolkacheva, G. A. 1995. 'Assessment of Possible Scales of Wind-Borne Salt Transport from the Exposed Area and Water Surface of the Aral Sea'. *Proceedings of SANIGMI* 151 (232): 6-13.

Tolkacheva, G. A. 2000. *Scientific and Methodological Foundations of Atmospheric Deposition Monitoring in the Central Asian Region*. SANIGMI. Tashkent.

Wæhler, Turid Austin, and Erik Sveberg Dietrichs. 2017. 'The Vanishing Aral Sea: Health Consequences of an Environmental Disaster'. *Tidsskrift for Den Norske Legeforening*, ahead of print, October 2. https://doi.org/10.4045/tidsskr.17.0597.

Wang, Wei, Alim Samat, Jilili Abuduwaili, Yongxiao Ge, Philippe De Maeyer, and Tim Van De Voorde. 2022. 'Temporal Characterization of Sand and Dust Storm Activity and Its Climatic and Terrestrial Drivers in the Aral Sea Region'. *Atmospheric Research* 275 (September): 106242. https://doi.org/10.1016/j.atmosres.2022.106242.

Xi, Xin, and Irina Sokolik. 2016. 'Quantifying the Anthropogenic Dust Emission from Agricultural Land Use and Desiccation of the Aral Sea in Central Asia: Anthropogenic Dust in Central Asia'. *Journal of Geophysical Research: Atmospheres* 121 (October). https://doi.org/10.1002/2016JD025556.

Xi, Xin, Jun Wang, Zhendong Lu, et al. 2025. 'Analysis of a Saline Dust Storm from the Aralkum Desert – Part 1: Consistency between Multisensor Satellite Aerosol Products'. *Atmospheric Chemistry and Physics* 25 (13): 7403–29. https://doi.org/10.5194/acp-25-7403-2025.

Yapiyev, Vadim, Andrew J. Wade, Maria Shahgedanova, Zarina Saidaliyeva, Azamat Madibekov, and Igor Severskiy. 2021. 'The Hydrochemistry and Water Quality of Glacierized Catchments in Central Asia: A Review of the Current Status and Anticipated Change'. *Journal of Hydrology: Regional Studies* 38 (December): 100960. https://doi.org/10.1016/j.ejrh.2021.100960.

Zender, Charles S., Huisheng Bian, and David Newman. 2003. 'Mineral Dust Entrainment and Deposition (DEAD) Model: Description and 1990s Dust Climatology'. *Journal of Geophysical Research: Atmospheres* 108 (D14): 2002JD002775. https://doi.org/10.1029/2002JD002775.

Zhang, L. 2001. 'A Size-Segregated Particle Dry Deposition Scheme for an Atmospheric Aerosol Module'. *Atmospheric Environment* 35 (3): 549–60. https://doi.org/10.1016/S1352-2310(00)00326-5.

Zhang, Zhuodong, Ralf Wieland, Matthias Reiche, et al. 2011. 'Wind Modelling for Wind Erosion Research by Open Source Computational Fluid Dynamics'. *Ecological Informatics* 6 (5): 316–24. https://doi.org/10.1016/j.ecoinf.2011.02.001.

Zobeck, T. M., N. C. Parker, S. Haskell, and K. Guoding. 2000. 'Scaling up from Field to Region for Wind Erosion Prediction Using a Field-Scale Wind Erosion Model and GIS'. *Agriculture, Ecosystems & Environment* 82 (1–3): 247–59. https://doi.org/10.1016/S0167-8809(00)00229-2.